Summer 2021

Design and evaluation of the 3D printed electromagnetic absorber built with conductive carbon-filled filament

Rui Mi

Department:

DESIGN AND EVALUATION OF THE 3D PRINTED ELECTROMAGNETIC ABSORBER BUILT WITH CONDUCTIVE CARBON-FILLED FILAMENT

by

RUI MI

A THESIS

Presented to the Graduate Faculty of the

MISSOURI UNIVERSITY OF SCIENCE AND TECHNOLOGY

In Partial Fulfillment of the Requirements for the Degree

MASTER OF SCIENCE

in

ELECTRICAL ENGINEERING

2021

Approved by:

Daryl G. Beetner, Advisor
Victor Khilkevich
DongHyun Kim

PUBLICATION THESIS OPTION

This thesis consists of the following one article, formatted in the style used by the Missouri University of Science and Technology.

Paper I: Pages 3-22 have been submitted to the EMC+SIPI & EMC Europe 2021 Conference in Glasgow, United Kingdom, in July 2021.

ABSTRACT

This research presents an application of the resistive frequency selective surface (FSS) fabricated with a 3D printed conductive material as an electromagnetic absorber for the EMI-reducing door. This solution allows to reduce radiated emissions of a router system. The resistive frequency selective surface has a three-layer structure. The top layer is a 3D printed FSS pattern, the middle layer is an air gap, and the bottom layer is a metal plane.

The first paper presents the methodology for manufacturing a frequency selective surface using the 3D printing technology, including the material characterization, design, fabrication, and evaluation.

The unpublished content presents the results of applying the 3D printed resistive frequency surface to a mock up of a router system. The prototype is evaluated in terms of the reflection coefficient and total radiated power measurements. After that it is attached to the EMI-reducing door and tested on the router system mock up.

ACKNOWLEDGMENTS

I would like to thank all the member from EMC Laboratory to help me achieve a one of most important step in my life.

Any word is meaningless when I appreciate the people who have had given me help.

This paper is based upon work supported partially by the National Science Foundation under Grant No. IIP-1916535.

TABLE OF CONTENTS

Page

SECTION

LIST OF ILLUSTRATIONS

Figure Page

PAPER I

SECTION

LIST OF TABLES

1. INTRODUCTION

EMI door is one of the commonly used shielding devices to provide an extra shielding performance for a large server rack for a router system. It could reduce the radiation emission from the device on the rack and passing the standard radiation emission test. However, due to the tendency of high speed and high-density, the present EMI door design may not be sufficient for the EMI compliance test.

Two major directions can be used to improve the performance of the EMI door: 1. Changing the design of the EMI door to create extra scattering to the radiation; 2. Adding electromagnetic lossy material inside the EMI door. However, increasing scattering effectiveness based on modifying the door structure is limited by the radiation power of the system. Therefore, considering the mechanical requirement of the router system, an electromagnetic absorber could be applying to the EMI door to further reduce the emissions.

The current commercial broadband electromagnetic absorbers do provide superior radiated emission reduction and a variety of choices. But it is generally built by high-density thick foam, fabric, or rubberized to achieve broadband absorption, which violates the thermal requirements in EMI door application. Besides, the cost of commercial broadband absorber material is not economic for the end-user.

Frequency selective surface (FSS) is one kind of single or multilayer of a periodic structure composed of period passive resonant unit [14]. This surface can show reflection or transmission at the resonance frequency. The resistive frequency selective surface absorber is consisting of FSS build by conductive material, a dielectric substrate, and a ground plane. The resistive FSS could design to resonates at the arbitrary frequency with relatively wide bandwidth, thin thickness, low cost. It is a preferred structure in the EMI door application.

Based on the various kind of conductive 3D printing material on the market, a flexible structures design, and easy tuning procedures, the 3D printed resistive FSS could provide the capability of the fastest rapid design, test, and redesign working flow. In Paper I, a novel 3D printed resistive FSS design flow is proposed, which includes the material characterization, FSS pattern design, 3D print fabrication, optimization, and validation.

In unpublished content, the resistive FSS designed for the router system working at 26.5 GHz is presented. The 3D printed prototype is evaluated on the router system.

PAPER

I. 3D PRINTED ELECTROMAGNETIC ABSORBER BUILT WITH CONDUCTIVE CARBON-FILLED FILAMENT

RUI MI
Department of Electrical and Computer Engineering
Missouri University of Science and Technology
Rolla, Missouri 65409–0050
Tel: 573–341–6622, Fax: 573–341–4115
Email: rmfd2@mst.edu

ABSTRACT

This article presents a methodology of manufacturing frequency selective surfaces (FSS) based on a 3D printed conductive material. The whole procedure including material characterization, design, fabrication, and evaluation is described. The FSS design is based on a three-layer structure. The first layer is a 3D printed lossy material, the second layer is an air gap, and the third layer is a ground plane. By changing the geometrical parameters of the 3D printed layer, it is possible to tune the frequency of the absorption band of the FSS.
Keywords: frequency selective surface, 3D printing, conductive lossy material, radiated emissions.

1. INTRODUCTION

EMI absorbers are commonly used to reduce radiated emissions from electronic devices. For most absorbers available on the market like rubberized lossy materials, foam-based lossy materials, ferrites, their absorption depends mainly on the electrical or magnetic

properties of the material. These products generally perform as broadband absorbers with wide absorption bandwidth. But their absorption performance might be insufficient for certain applications.

The frequency selective surfaces (FSS) are alternatives to broadband absorbers allowing to increase the absorption at a certain frequency due to intrinsic resonances of the structure [1].

Frequency selective surfaces are periodic structures composed of passive resonant units. At the resonance frequency the absorptive FSS will have low reflectivity [2]. If the FSS is built with a lossy material in front of the metal plate (Figure 1), it could be a good narrowband absorber [3]. Properly designed lossy FSS should resonate at a desired frequency with relatively wide bandwidth, and low cost is preferred.

The resonance frequency of the FSS depends on the EM properties of materials, dimensions of the structure and in general is specific to the incident angle of the exciting plane wave [2]. The PCB technology is a most widely used method to manufacture the FSS [4][5]. It could provide good accuracy and a mechanically stable design.

However, compared with FSS manufactured on PCB, the 3D printed structures could provide capabilities of a faster design, test, and optimization with lower cost and are more suitable to implement non-planar surfaces.

This is not the first-time application of the 3D printing technology for FSS design and manufacturing is proposed. 3D printed FSS are reported in [6], [7] and [8]. In [7], the FSS performed based on an all-dielectric structure. In [8], the FSS structure is built by using a standard polylactic acid (PLA) filament with conductive paint applied to the surface to make it conductive.

There is a wide variety of composite materials for 3D printing on the market. Among other types there are filaments with conductive inclusions – metals and carbon, which can exhibit properties desirable for electromagnetic absorbers (high dielectric constant, high loss). In [6] several FSS were successfully implemented in the frequency range around 10

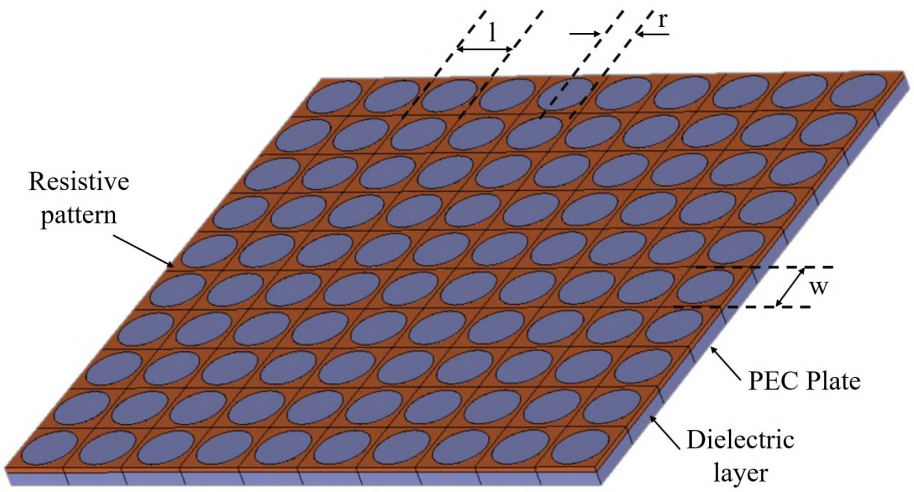

Figure 1. Basic structure of the FSS absorber [3].

GHz using metal-filled PLA filaments. The metal-filled filaments have typically 80%-90% mass fraction of metal inclusions (their intended application is sintering of 3D printed objects to produce solid metal parts) and the FSS made with these materials are relatively heavy. For example, the copper-filled PLA [9] used in [6] has density of $4\,g/cm^3$. On the other hand, a carbon-filled PLA available at Proto-pasta [10] has density of just $1.24\,g/cm^3$ (close to density of standard PLA). For cost considerations, the copper-filled PLA has twice the price compared with the carbon-filled PLA with same volume. Aluminum-filled PLA has similar density to normal PLA (around $1.5\,g/cm^3$), but due to the manufacturing difficulties, its cost is even higher compared to other metal-filled filaments. In general, the carbon-filled PLA is a lighter and more cost-effective material compared with metal-filled filaments. To demonstrate a possibility of designing an FSS using the carbon-filled PLA, a complete 3D printed FSS design flow is proposed, which includes material characterization, FSS pattern design, prototype 3D printing, optimization, and validation.

2. DESIGN FLOW

Figure 2 shows the flowchart of proposed FSS design method. Firstly, the properties of the 3D printing material to be used are characterized. Next the geometry of the FSS structure is optimized using a 3D solver to match the desired frequency response. The sensitivity of the frequency response to the incident angle is checked. The final design is determined once the desired performance is achieved.

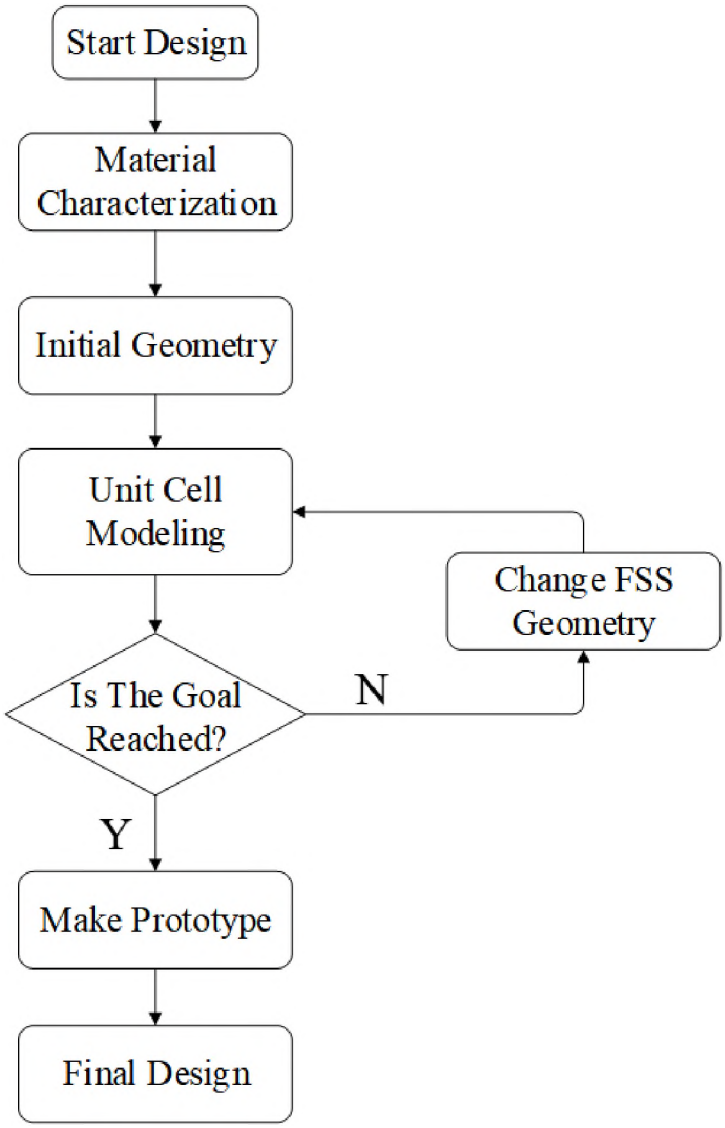

Figure 2. FSS Design Workflow.

3. MATERIAL CHARACTERIZATION

The material characterization setup is based on the airline method implemented in the Keysight's 85071 material characterization software [11]. A coaxial 7 mm airline (800 MHz to 18 GHz) is used for characterization of the material properties of dielectric samples (Figure 3) [12]. Figure 3 shows the coaxial setup along with the 3D printed dielectric samples.

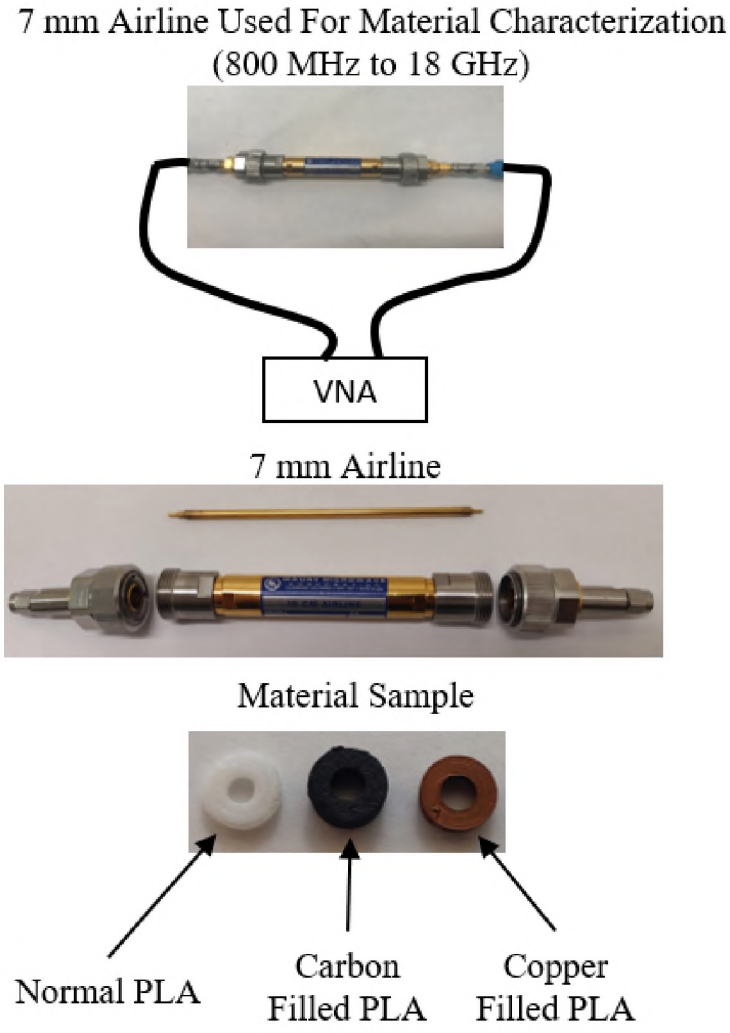

Figure 3. Material Characterization Setup With 7 mm Airline For 800 MHz to 18 GHz.

After calibrating the setup (a TRL calibration is usually applied), the transmission and reflection coefficients of the medium with the inserted samples are measured. The software calculates the complex permittivity and permeability of the samples. Samples of three materials were printed and characterized: 1. ColorFabb copper-filled PLA [9]; 2. Proto-pasta electrically conductive PLA (CDP11705, Carbon-filled PLA) [10]; 3. Generic PLA. The 7 mm airline-measured material parameter between 800 MHz and 18 GHz results are presented in Figure 4.

As can be seen from the plot, both permittivity and dielectric loss tangent of the carbon-filed PLA is higher compared to the copper-filled PLA (the electric loss tangent is significantly higher), making it quite appealing for electromagnetic absorber applications. The dielectric constant of the PLA filaments is close to the expected value (2.7) [13].

4. DESING AND SIMULATION OF RESISTIVE FSS

The proposed FSS design, which follows [6], consists of three layers: the top layer is the FSS pattern, the middle layer is the homogenous dielectric, and the bottom layer is the metal plate. The FSS on the top layer is 3D printed using the lossy carbon-filled PLA. The middle dielectric layer is an air gap. The resistive lossy FSS structure is mounted on the metal surface which constitutes the third layer.

The top-layer resistive FSS pattern is based on a simple periodic structure with a circular aperture in the unit cell [6]. Figure 5 demonstrates the dimensions of the unit cell which is characterized by the thickness t and width l. The middle of the square contains an aperture of radius r. the whole FSS surface is created by a periodic repetition of the unit cell. If the material of the FSS structure is chosen, the structure has only four design variables: the unit cell size l, the radius r for aperture, the thickness of FSS t_{FSS}, and the thickness of air gap t_{gap}. Compared with other FSS patterns with more complex structure, the simplicity of the structure in Figure 5 is appealing from the manufacturing point of view.

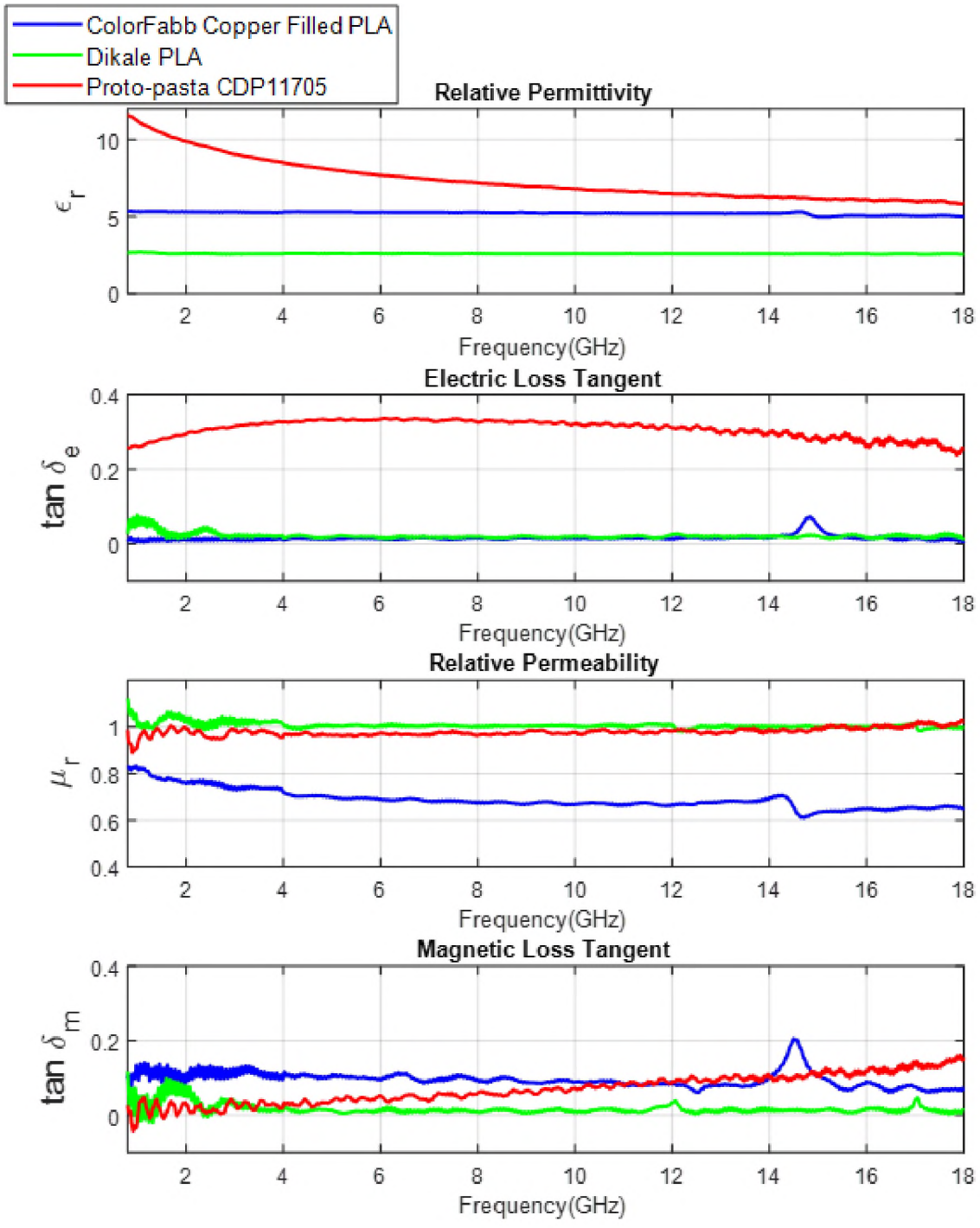

Figure 4. Relative Permittivity, Permeability, Electrical Loss Tangent and Magnetic Loss Tangent of the Filament Materials Measured By 7 MM Airline (800 MHz to 18 GHz).

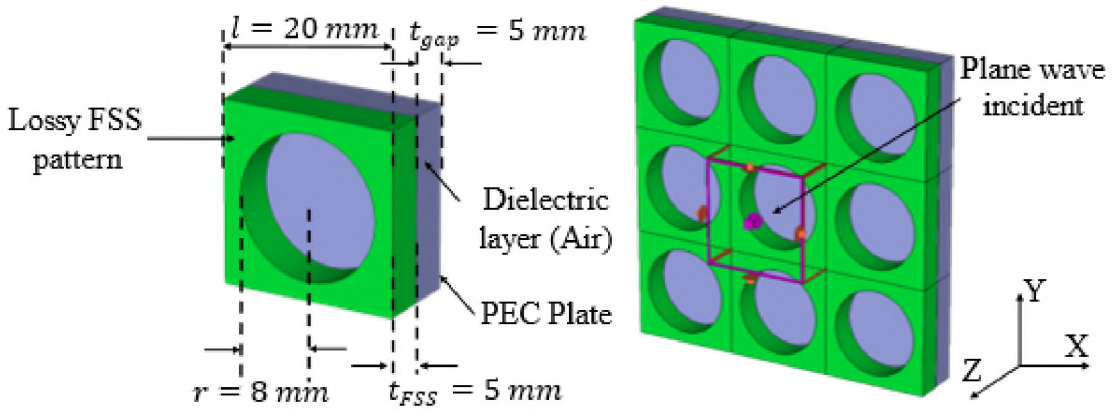

Figure 5. FSS Structure Designed for Frequency Range Between 12 GHz and 13 GHz.

To model the structure, a full-wave frequency domain solver with periodic boundary conditions producing a structure infinite in the XY plane was used. The excitation source is a plane wave propagating along the Z axis which corresponds the first Floquet mode.

Based on the absorption band of interest (12 GHz – 13 GHz), the unit cell's initial dimension is determined according to recommendations in [2]: the unit cell size is 1 wavelength, and the radius of the aperture is $\frac{1}{4}$ wavelength (the wavelength is calculated at 12.5 GHz in air). The thickness of the FSS pattern is set equal to the air gap. During the design procedure the resonance frequency of the FSS first is adjusted by sweeping the unit cell's and aperture sizes withing a relatively large range (± 10 mm with 1 mm per step).

Once the resonate frequency is close to the goal, optimization is applied to fine-tune the structure's parameters. At this stage, the geometrical parameters are allowed to change in a small range (± 2 mm).

In a wide frequency range (1 GHz to 18 GHz), multiple resonances of the reflection coefficient can be observed. The higher order resonances are more sensitive to the physical dimensions and the incident angle of the plane wave. At the same time, the first order

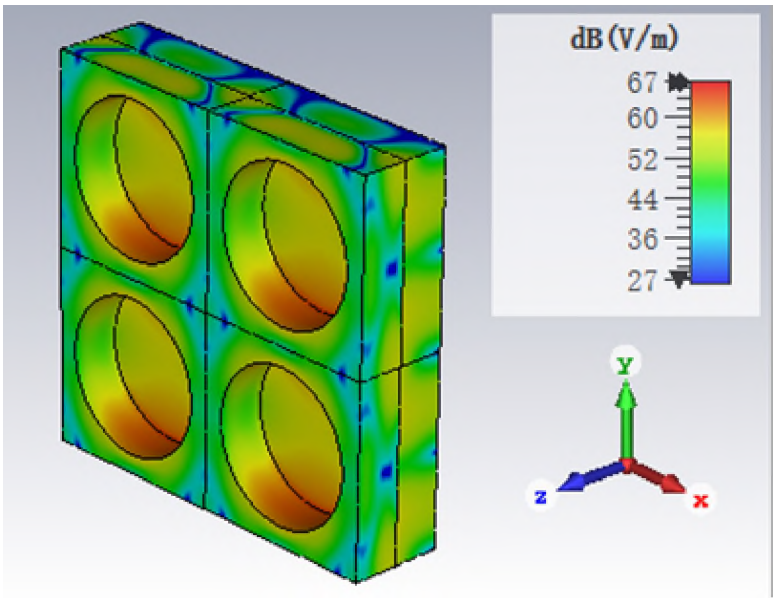

Figure 6. E-field at 12.37 GHz FSS Unit Cell.

resonance cannot provide more than 25 dB reflection reduction (at least according to simulation). Therefore in order to achieve large absorption (at the expense of increased sensitivity to the incident angle), second order resonance was selected to design the FSS.

Figure 6 and Figure 7 shows the E-field and current density at designed resonate frequency of the optimized structure.

Figure 8 shows the reflection coefficient of the infinite FSS with dimensions listed in Figure 5 illuminated by a plane wave at different angles. When the incident wave directly projects on the FSS, it could provide over 40 dB reduction at the resonance frequency. For oblique incidence angles attenuation reduces but remains at least -8 dB for angles not exceeding 40 degrees in the frequency range between 10 GHz to 14 GHz.

Once the structure met the desired working frequency with decent absorption performance the structure was 3D printed for further testing.

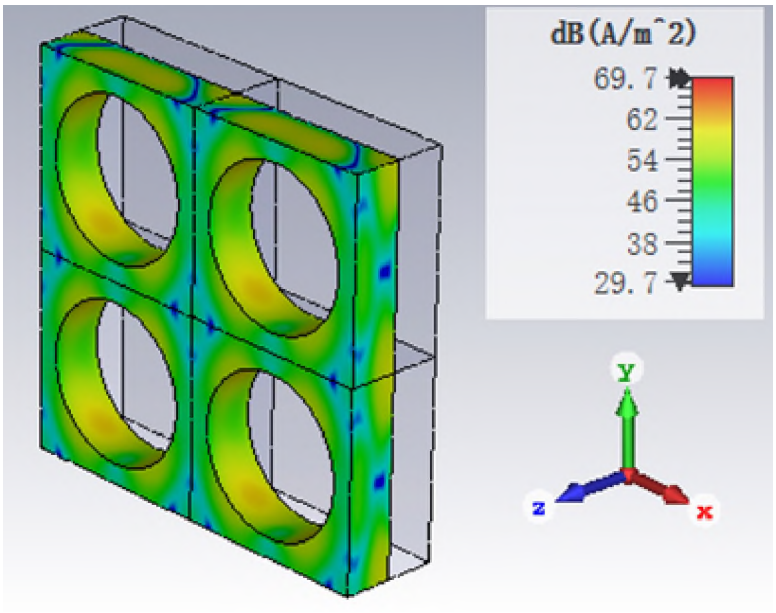

Figure 7. Current Density at 12.37 GHz FSS Unit Cell.

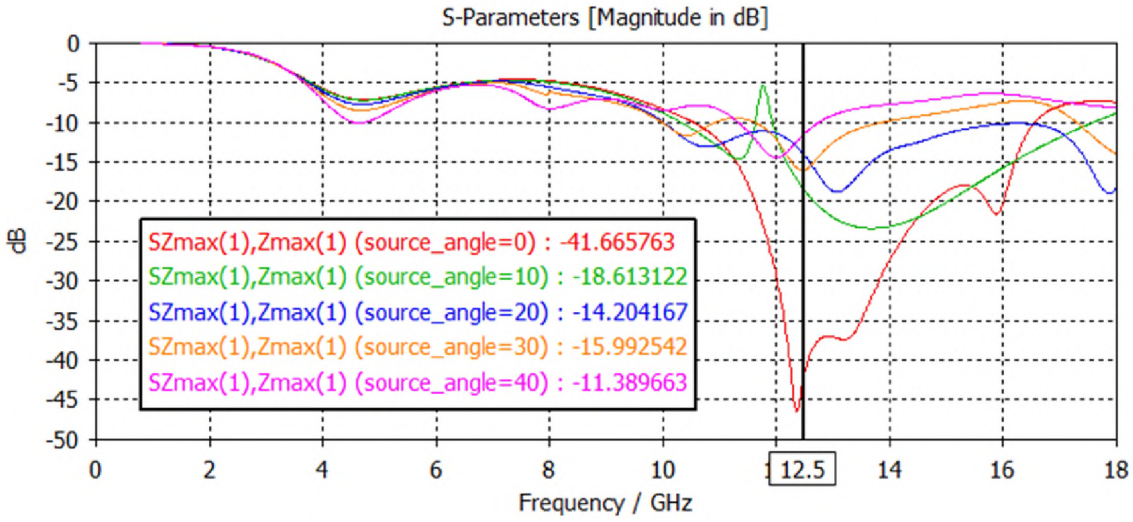

Figure 8. Simulated 12.5 GHz FSS Reflectivity for Different Incident Angles.

5. MANUFACTURE AND VALIDATION

5.1. 3D PRINTED PROTOTYPE MANUFACTURE

Two structures were printed for experimental evaluation. The first one is a 5 cm by 5 cm square solid pad with 5mm thickness printed by carbon-filled PLA (Figure 9).

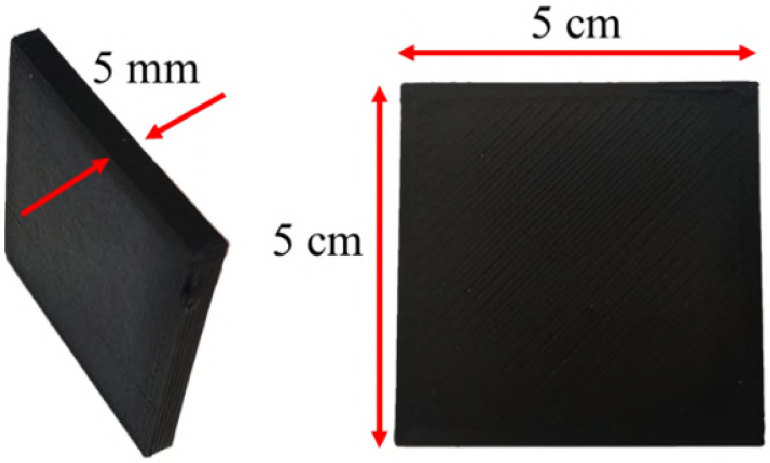

Figure 9. 3D Printed Solid Pad.

The second sample is printed as a 5 by 5 cell FSS pattern according to the dimensions determined in the previous section (Figure 5). To maintain the airgap between the periodic dielectric layer and the metal ground plate, 5 mm spacers on the back side of FSS prototype are added (Figure 10).

5.2. REFLECTION COEFFICIENT MEASUREMENT

To evaluate the performance of the 3D printed resistive FSS a synthetic aperture radar (SAR) is used. Its implementation is based on the Emission source microscopy (ESM) technique that is used to locate the radiation sources by measuring the electromagnetic field on a planar surface [14]. The SAR setup is shown in Figure 11. By measuring the reflection coefficient of the horn antenna moved on the scan plane at 10 cm above the FSS and applying the SAR algorithm, the FSS performance can be evaluated.

To eliminate the influence of unwanted reflections (i.e. to increase the dynamic range of the measurement), the measured antenna reflection coefficient is gated in the time domain [15]. The gating window is determined by measuring the reflection over the metal plate as demonstrated in Figure 12. An example of the raw and gated frequency domain

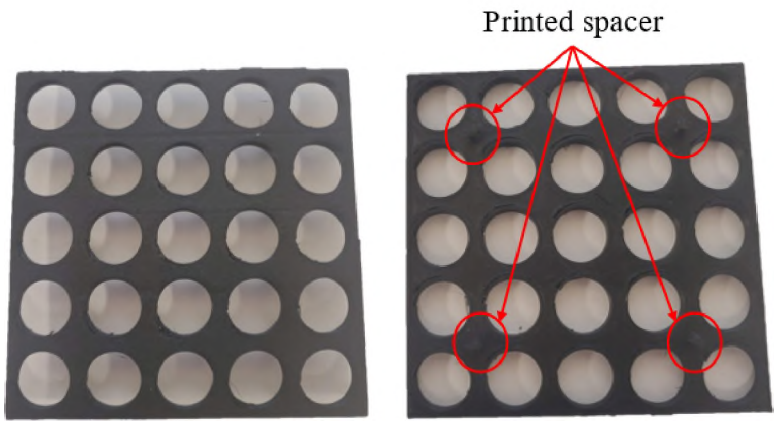

Figure 10. 3D Printed FSS Prototype Designed for Frequency Range Between 12 GHz and 13 GHz.

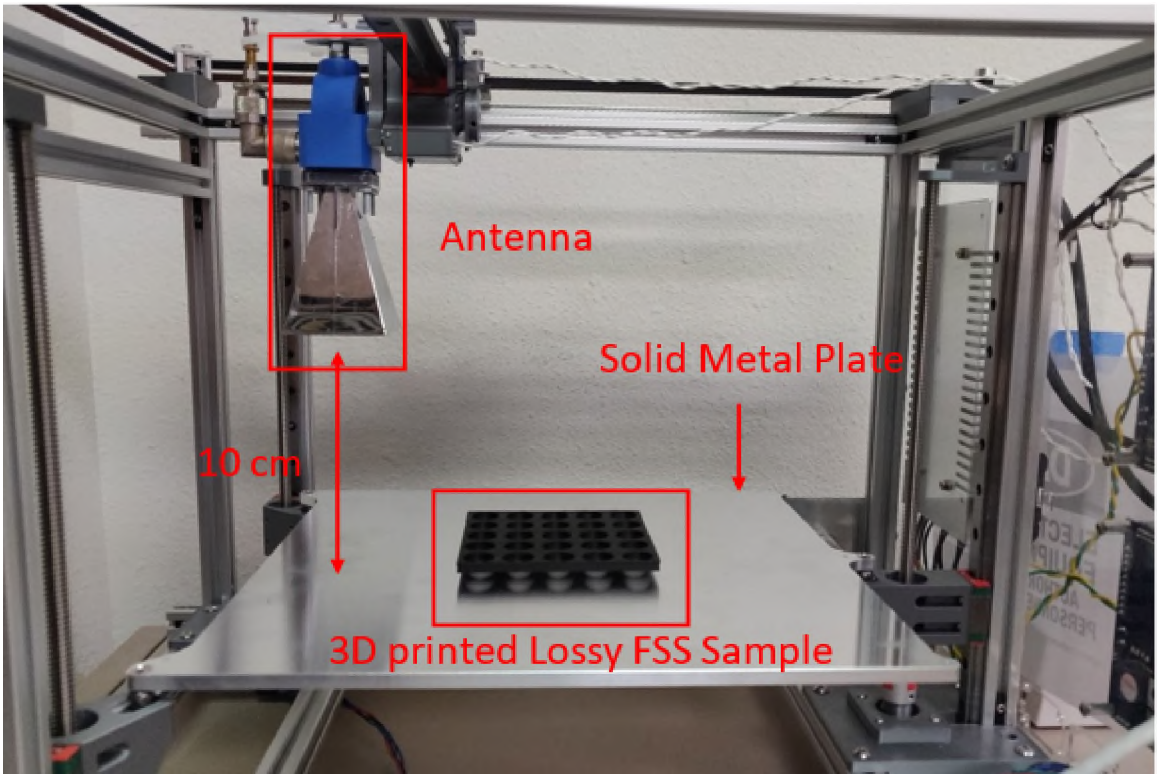

Figure 11. SAR Setup for FSS Performance Evaluation.

reflection coefficients measured at one location over the FSS is shown in Figure 13. As can be seen, as opposed to the raw reflection coefficient, the gated one clearly shows the absorption band.

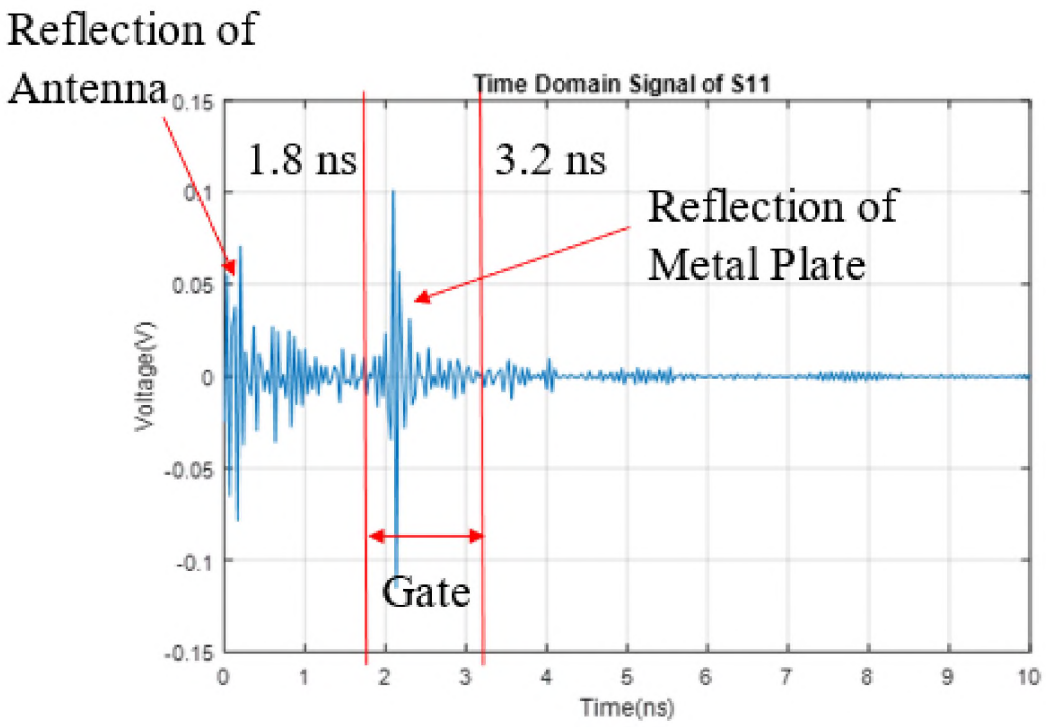

Figure 12. Gating Method to Remove the Aperture Reflection from the Data.

Table 1. Reflection Coefficient of Different Material at 11.5 GHz.

Material	Reflectivity, dB			
	Max	Min	Mean	Mean reflection coefficient relative to the metal plate
Metal Plate	-15.5	-18.5	-17.1	0
Solid 3D Printed Pad	-19.1	-26.1	-20.6	-3.46
3D Printed FSS	-19.1	-67.7	-36.3	-19.2
Commercial Absorber	-22.8	-49.4	-30.9	-13.8

Compared to measuring the reflection coefficient at one location (as in Figure 13), the SAR scan allows to obtain an image of the sample with high spatial resolution, reducing the influence of the edge effects due to a relatively small size of the samples used in the study. In the images in the following figures the color represents the magnitude of

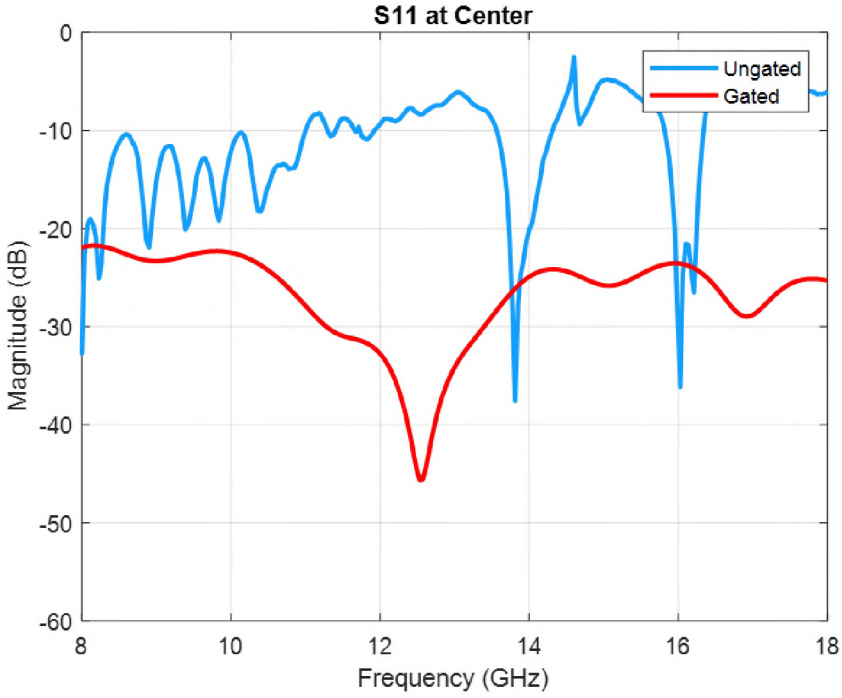

Figure 13. Raw and Gated FD Reflection Coefficient Curves Measured Over the Center of the FSS.

the reflection coefficient at 11.5 GHz. Three samples are compared: solid carbon-filled PLA pad (Figure 15), 3D printed FSS designed working between 12 GHz to 13 GHz (Figure 16) and a commercial foam absorber (Figure 17. Since the reflection coefficient is not uniformly distributed even within nominally uniform surfaces (this happened because of the SAR aperture diffraction) and is especially non-uniform for the FSS, rectangular regions were defined in all images, and the minimum, maximum and averages values of the absolute value of the reflectivity over the entire frequency range were calculated. This allows to perform a more accurate comparison and avoid influence of local variations. The values of reflection coefficient at 11.5 GHz (maximum absorption frequency for the FSS) are given in Table 1. By using the reflection coefficient of the metal plate as a reference (0 dB reflection) the absolute reflectivity of other samples is determined.

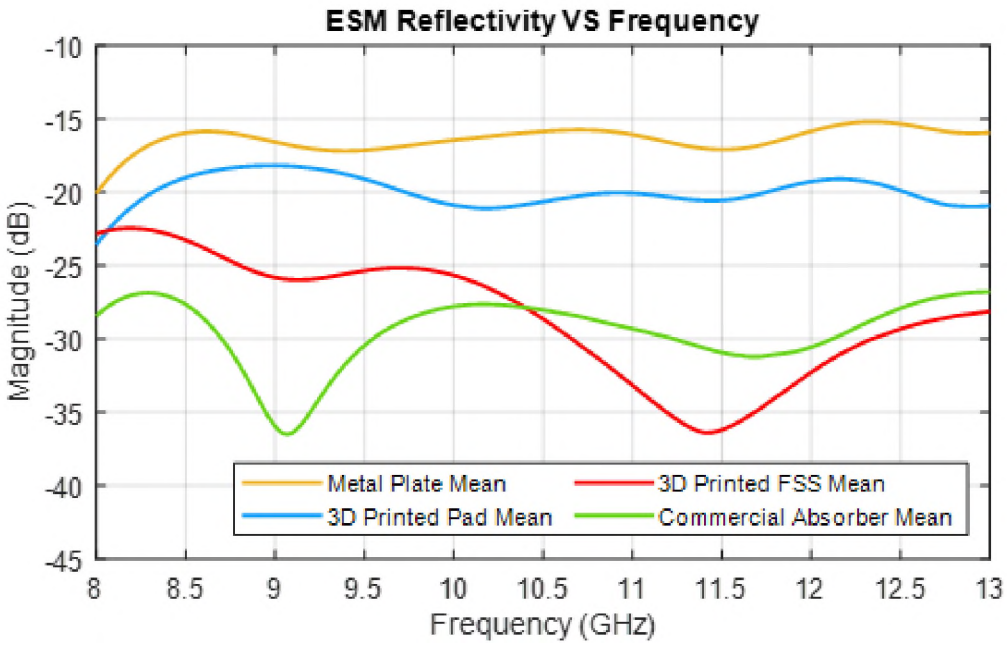

Figure 14. Mean Value of Reflectivity at the Selected Area of the Samples Obtained by the SAR Scan.

Compared with the reflection of the printed solid pad (Figure 15), the 3D printed lossy FSS for 12 GHz to 13 GHz (Figure 16) could provide extra 16 dB reduction at 11.5 GHz which even exceeds the performance of the commercial absorber(Figure 17).

The SAR scanned different material's mean value of reflectivity in the entire frequency range is presented in Figure 14. As can be seen, the 3D printed FSS provides the best narrowband absorption reaching 19.2 dB reduction at 11.5 GHz. Comparing to just 3.46 dB reduction of the solid carbon-dilled PLA piece this is a significant improvement. The reflection of the commercial absorber at 11.5 GHz is -14 dB. Due to the tolerance of 3D printing and, more importantly, limited accuracy of the material parameter measurements, the resonate frequency of the printed FSS is shifted relative to the design (Figure 8).

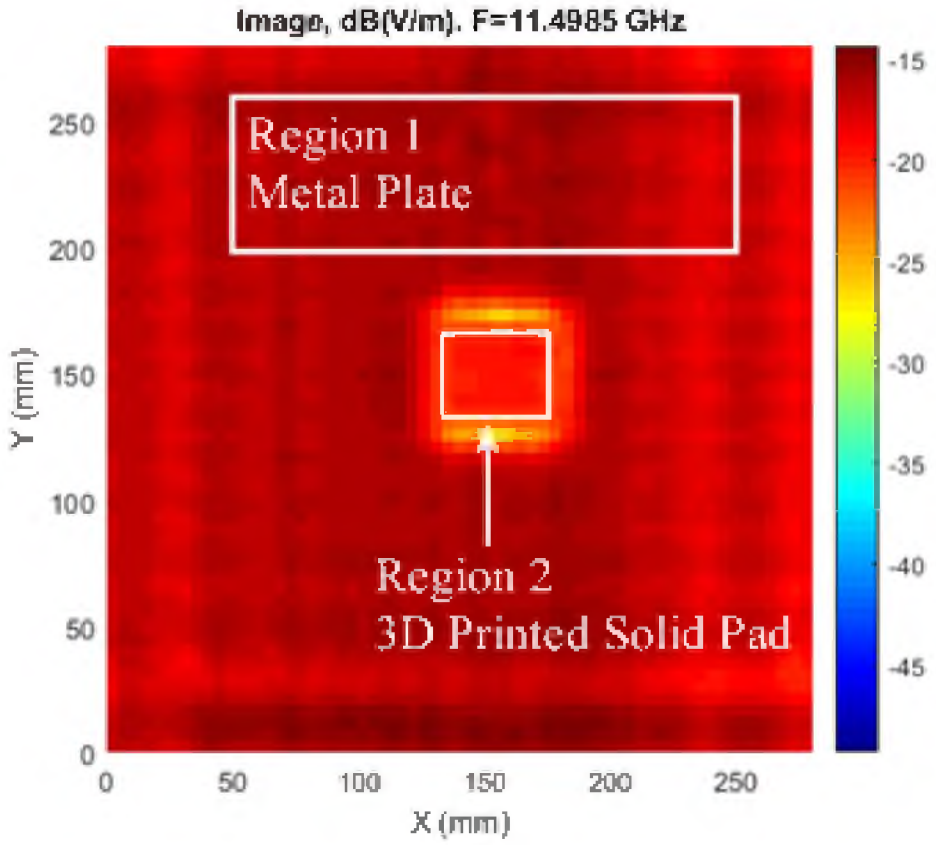

Figure 15. 3D Printed Solid Pad Reflectivity at 11.5 GHz. Region 1 Represent the Averaging Region of Metal Plate. Region 2 Represent the Averaging Region of 3D Printed Solid Pad.

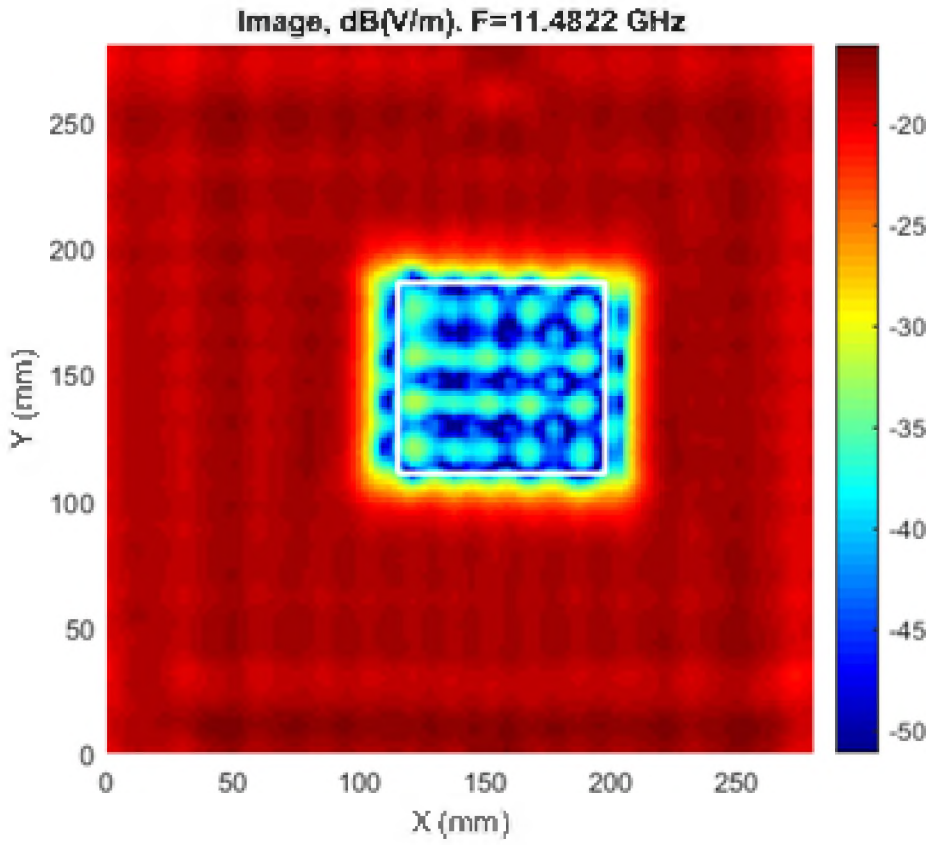

Figure 16. 3D Printed FSS Prototype Reflectivity at 11.5 GHz. White box Represents the Averaging Region.

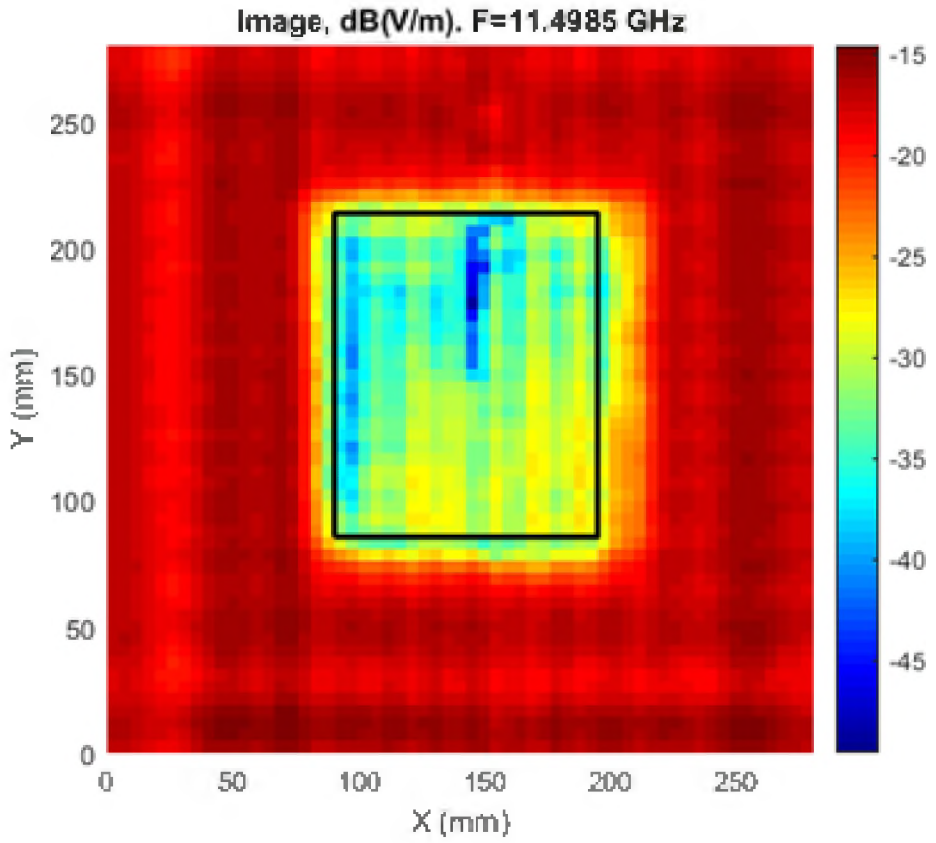

Figure 17. Commercial Broadband Absorber Reflectivity at 11.5 GHz. Black Box Represents the Averaging Region.

6. CONCLUSIONS

This paper introduced a methodology for design and reflectivity measurement for a resistive FSS 3D printed using conductive carbon-filled material. Because it is a simple periodic structure, it is easily to model and tune at the design stage allowing to create structures targeting arbitrary frequencies relatively easily. SAR scan allows to obtain reflectivity images and accurately evaluate the FSS performance.

The current design still has several problems which need to be addressed. The first problem is the sensitivity of the absorption to the incident angle. Alternative FSS patterns (like annular rings) might provide better performance in this regard. Another problem is the overall thickness of the proposed FSS structure (10 mm), which limits its applicability. At same time, resonate frequency of the prototype has a 1 GHz shift compared with simulation results. Possible reasons for this include inaccuracies of the material parameter measurements and 3D printing geometrical tolerances which require additional investigation.

ACKNOWLEDGMENTS

This paper is based upon work supported partially by the National Science Foundation under Grant No. IIP-1916535.

REFERENCES

[1] Filippo Costa, Agostino Monorchio, and Giuliano Manara. Analysis and design of ultra thin electromagnetic absorbers comprising resistively loaded high impedance surfaces. *IEEE Transactions on Antennas and Propagation*, 58(5):1551–1558, 2010.

[2] Ben A Munk. *Frequency selective surfaces: theory and design*. John Wiley & Sons, 2005.

[3] MWB Silva, ALPS Campos, and LC Kretly. Design of thin microwave absorbers using lossy frequency selective surfaces. *Microwave and Optical Technology Letters*, 57(4):928–933, 2015.

[4] Xian Qi Lin, Peng Mei, Peng Cheng Zhang, Zhi Zhang David Chen, and Yong Fan. Development of a resistor-loaded ultrawideband absorber with antenna reciprocity. *IEEE Transactions on Antennas and Propagation*, 64(11):4910–4913, 2016.

[5] Qiang Chen, Di Sang, Min Guo, and Yunqi Fu. Frequency-selective rasorber with interabsorption band transparent window and interdigital resonator. *IEEE Transactions on Antennas and Propagation*, 66(8):4105–4114, 2018.

[6] R Kronberger and Volker Wienstroer. 3d-printed fss using printing filaments with enclosed metal particles. In *2017 Progress in Electromagnetics Research Symposium-Fall (PIERS-FALL)*, pages 808–811. IEEE, 2017.

[7] Jay H Barton, Cesar R Garcia, Eric A Berry, Rodolfo Salas, and Raymond C Rumpf. 3-d printed all-dielectric frequency selective surface with large bandwidth and field of view. *IEEE transactions on antennas and propagation*, 63(3):1032–1039, 2015.

[8] Saptarshi Ghosh and Sungjoon Lim. A miniaturized bandpass frequency selective surface exploiting three-dimensional printing technique. *IEEE Antennas and Wireless Propagation Letters*, 18(7):1322–1326, 2019.

[9] ColorFabb. Copperfill, 2021. URL `https://colorfabb.com/copperfill`.

[10] Protopasta. Electrically conductive composite pla, 2021. URL `https://www.proto-pasta.com/products/conductive-pla`.

[11] Keysight. *85071B Materials Measurement Software User's Manual (Apr93)*, 1993.

[12] Michel Joussemet. Novel devices and material characterization at mm wave and terahertz. Technical report, 2010.

[13] Jaroslav Zechmeister and Jaroslav Lacik. Complex relative permittivity measurement of selected 3d-printed materials up to 10 ghz. In *2019 Conference on Microwave Techniques (COMITE)*, pages 1–4. IEEE, 2019.

[14] Pratik Maheshwari, Victor Khilkevich, David Pommerenke, Hamed Kajbaf, and Jin Min. Application of emission source microscopy technique to emi source localization above 5 ghz. In *2014 IEEE International Symposium on Electromagnetic Compatibility (EMC)*, pages 7–11. IEEE, 2014.

[15] Bruce Archambeault, Samuel Connor, and JC Diepenbrock. Time domain gating of frequency domain s-parameter data to remove connector end effects for pcb and cable applications. In *2006 IEEE International Symposium on Electromagnetic Compatibility, 2006. EMC 2006.*, volume 1, pages 199–202. IEEE, 2006.

SECTION

2. UNPUBLISHED CONTENT

2.1. MATERIAL CHARACTERIZATION FOR 18 GHZ TO 26.5 GHZ

The material property of 3D printing filaments measured by 7 mm airline is between 800 MHz to 18 GHz.The absorption frequency of the router system is 26.5 GHz, the material property of 3D printing filaments needs to be tested between 18 GHz to 26.5 GHz. The material characterization setup is based on Keysight's 86071 material characterization software [8] present in [13].

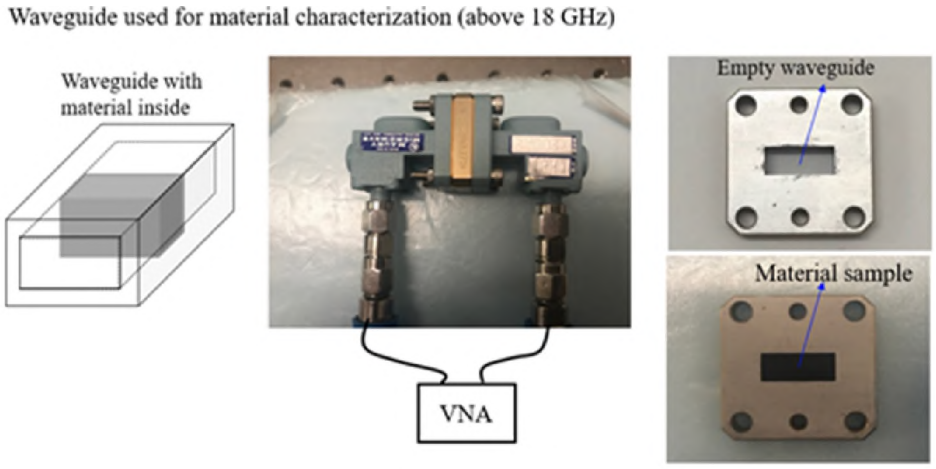

Figure 2.1. Material Characterization Setup With WR-42 Waveguide For 18 GHz to 26.5 GHz.

The Figure 2.1 shown the material characterization setup use WR-42 waveguide instead of 7 mm airline which could measure the material property between 18 GHz to 26.5 GHz. The sample we test is ColorFabb copper-filled PLA [4] and Proto-pasta electrically conductive PLA (CDP11705, Carbon-filled PLA) [15]. The material parameter measurement results are presented in Figure 2.2.

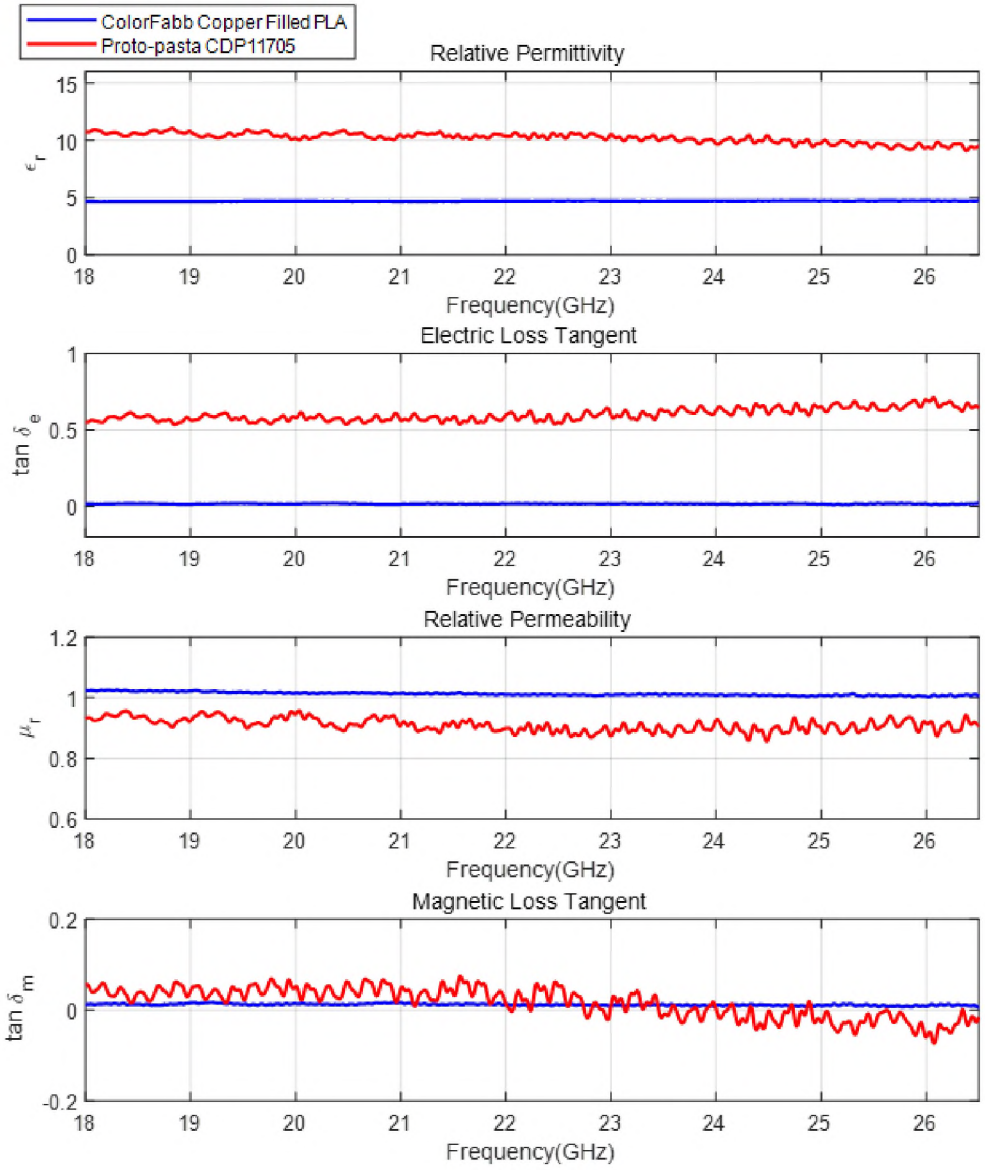

Figure 2.2. Relative Permittivity, Permeability, Electrical Loss Tangent and Magnetic Loss Tangent of the Filament Materials Measured By WR-42 Waveguide (18 GHz to 26.5 GHz).

By compare the material parameter measured between 1 GHz to 18 GHz [13], the material parameter of Proto-pasta electrically conductive PLA measured between 18 GHz to 26.5 GHz has more consistent relative permittivity value(10). The carbon-filled PLA still has higher relative permittivity and electric loss tangent then copper-filled PLA. It still will be the material for new lossy FSS design.

2.2. CIRCULAR APERTURE FSS PATTERN DESIGNED FOR 26 GHZ TO 27 GHZ.

With the same circular aperture FSS pattern in [13], by repeating the previous procedure, it could be designed to resonate at different frequency range. In this case, the target resonate frequency has been set at 26.5 GHz.

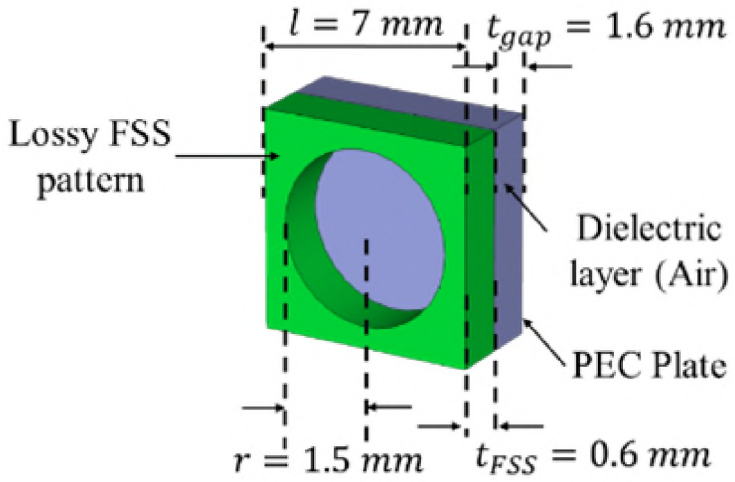

Figure 2.3. FSS Structure Designed for Frequency Range Between 26 GHz and 27 GHz.

The Figure 2.3 is showing the updated geometry designed to resonate at 26.5 GHz.

Figure 2.4 shows the reflection coefficient of the infinite FSS with dimensions listed in Figure 2.3 illuminated by a plane wave at different angles. When the incident wave directly projects on the FSS, it could provide over 30 dB reduction at the resonance frequency. For oblique incidence angles attenuation reduces but remains at least -8 dB for angles not exceeding 40 degrees in the frequency range between 21 GHz to 35 GHz.

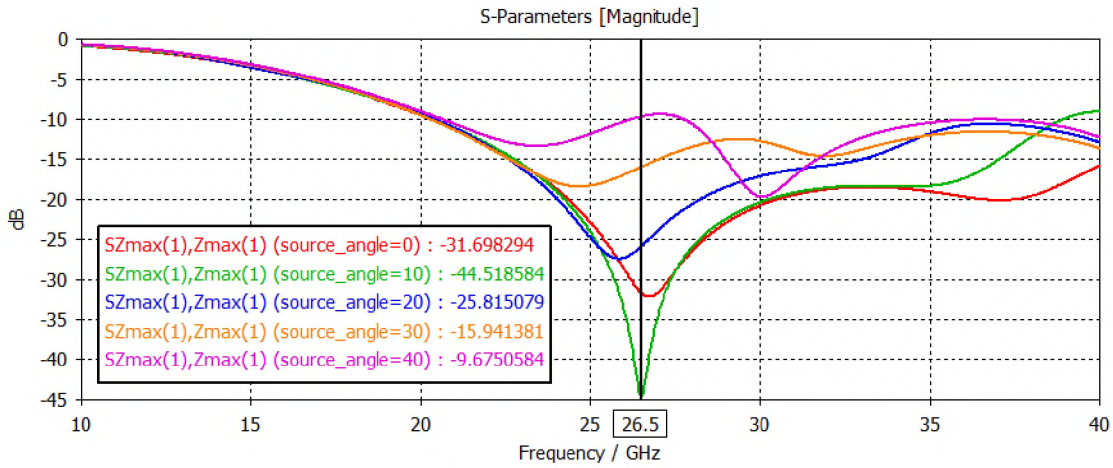

Figure 2.4. Simulated 26.5 GHz FSS Reflectivity for Different Incident Angles.

Since the updated 26.5 GHz FSS structure is using the first order resonance for absorption, it would not provide as higher reduction at resonance frequency as the second order resonance would. At the same time when applying a plane wave with different incident angle, the first order resonance of the FSS pattern has a more stable resonance frequency and wider reduction frequency range than the second order resonance.

2.3. MANUFACTURE AND VALIDATION FOR RESISTIVE FSS DESIGNED FOR 26.5 GHZ

2.3.1. 3D Printed Prototype. Based on optimization results in simulation, the prototype of 3D printed FSS designed for the frequency range between 26 GHz to 27 GHz has been made. This prototype is printed as a 14 by 14 cell FSS pattern according to the dimensions determined in the (Figure 2.3). To maintain the airgap between the periodic dielectric layer and the metal ground plate, 1.6 mm spacers on the back side of FSS prototype are added (Figure 2.5).

2.3.2. Reflection Coefficient Measurement. Based on the reflection coefficient measurement presented in [13], the 3D printed FSS prototype designed for 26.5 GHz is been test. The Figure 2.7 shown the reflectivity of the lossy FSS prototype has around 5

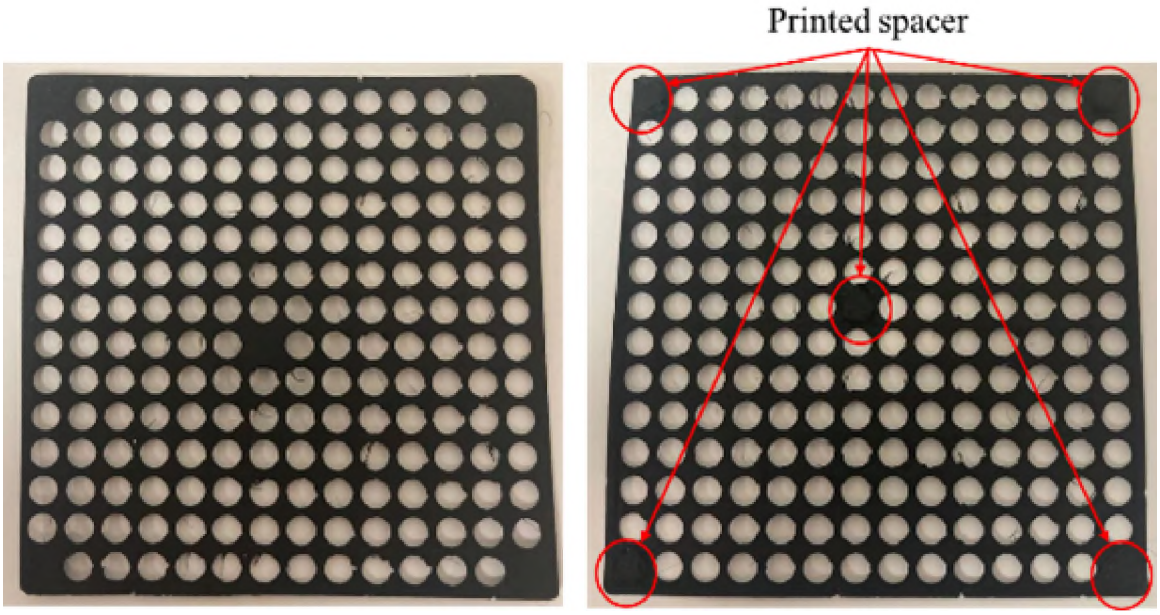

Figure 2.5. 3D Printed FSS Prototype Designed for Frequency Range Between 26 GHz and 27 GHz.

dB reduction at 26.5 GHz. The Figure 2.6 shown the mean value of reflectivity of the lossy FSS prototype between 18 GHz to 28 GHz. The black box in Figure 2.7 represents the average region of the mean value of reflectivity. The lossy FSS prototype design for 26.5 GHz could provide a 5 dB reduction between 22 GHz to 26 GHz.

2.3.3. Total Radiation Power Measurement. The total radiation power (TRP) measurement in reverberation tent could be used to characterize the absorption performance of the lossy material [11]. In the reverberation tent, two antennas are facing opposite directions, one is the transmitter antenna, another one is the receiving antenna (Figure 2.8). Before evaluating the resistive FSS, the dynamic range of the setup is checked by measuring the noise floor of the setup and coupling between the antennas without any absorbers. The TRP is measure by averaging amplitude of coupling between the antennas over multiple VNA sweeps while randomly shaking the tent walls: $TRP = |S_{21}|^2$. When characterizing the designed lossy FSS, the transmitted antenna is mounted facing the metal box covered

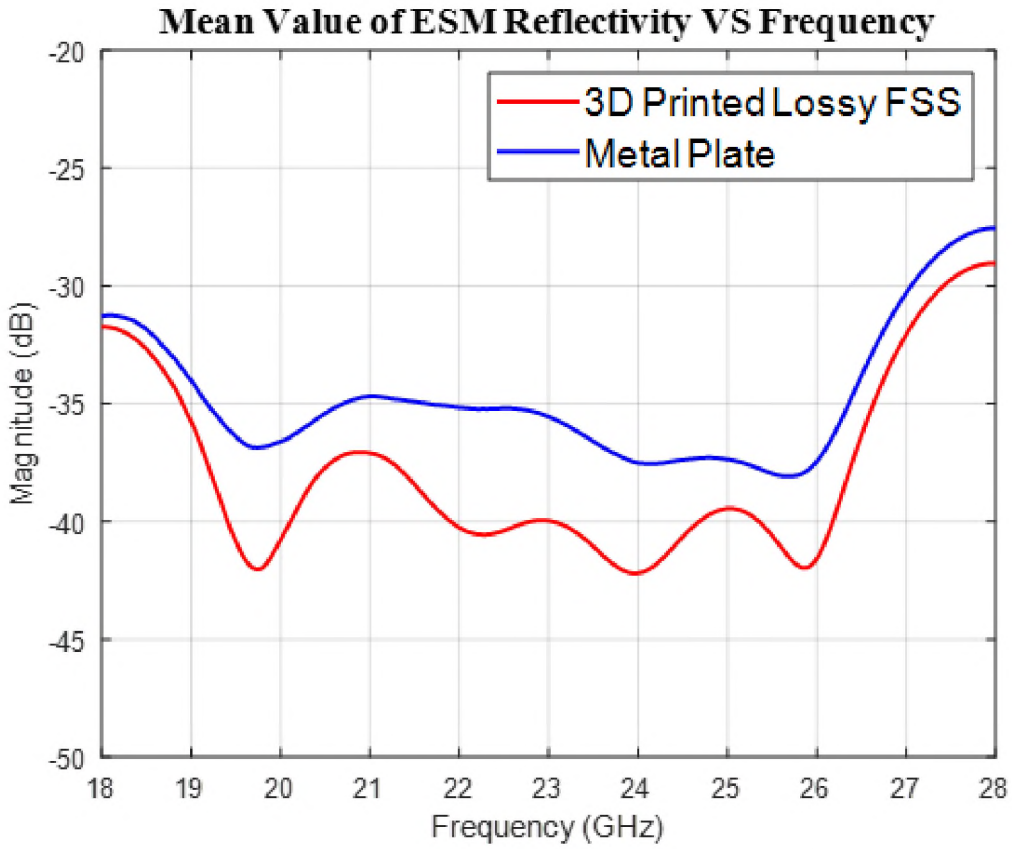

Figure 2.6. Mean Value of Reflectivity at the Selected Area of the Samples Obtained by the SAR Scan for Frequency Range Between 18 GHz and 28 GHz.

by lossy FSS inside. By comparing the coupling between the antennas measured with and without the absorber, the absorption rate of the lossy FSS is determined. In this setup the 3D printed FSS prototype which is designed to work between 26 GHz and 27 GHz has been test. The TRP measurements results showing Figure 2.9.By comparing with a no absorber case, it is showing a 6 dB reduction at the resonance frequency. Besides this, a commercial absorber (carbon-loaded polyurethane foam) was evaluated. A comparison showed that the 3D printed FSS prototype designed working between 26 GHz and 27 GHz has a similar absorption performance in terms of the TRP as the commercial absorber.

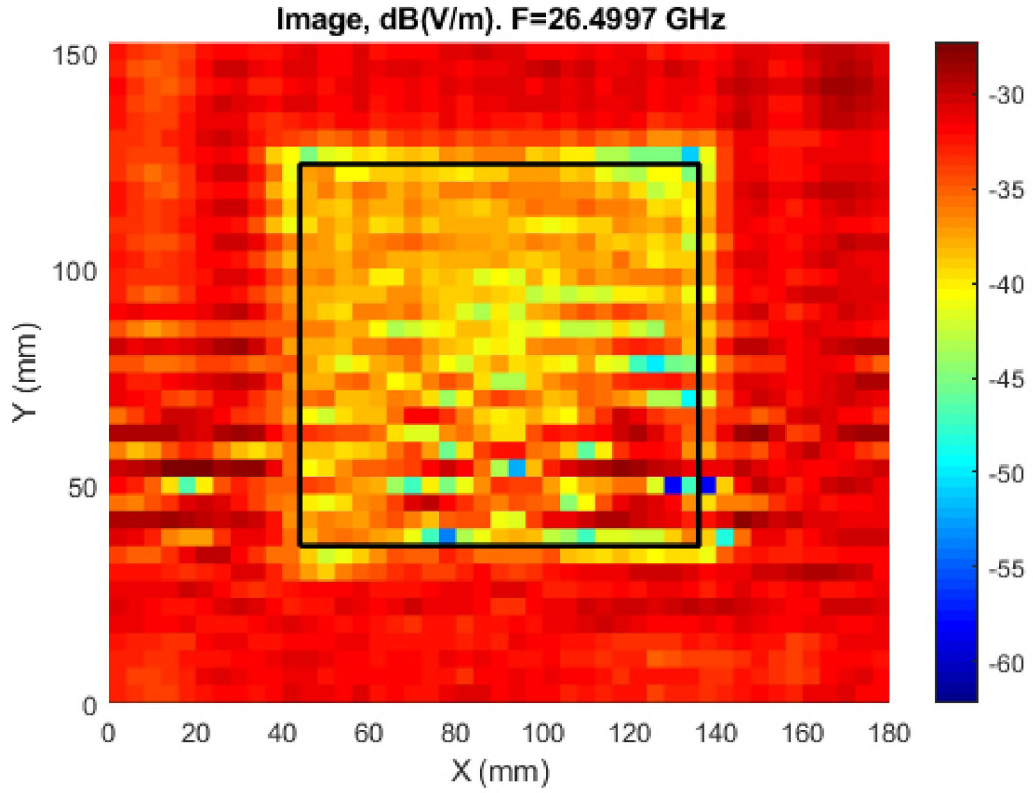

Figure 2.7. 3D Printed FSS Prototype Reflectivity at 26.5 GHz. Black Box Represents the Averaging Region.

2.3.4. Application Validation. To properly evaluate the effectiveness of the 3D printed FSS based on conductive filaments, it is essential to validate the 3D printed prototype in the actual application environment. The actual system under test is the router system loaded with line cards. EMI door is a solution to reduce the emission of the system and helps it pass the compliance test. Adding the lossy material inside the EMI door could provide extra attenuation.

The mockup of a router system rack is represented in Figure 2.10. The metal chassis with a custom-made waveguide source represents the server rack with a router installed.

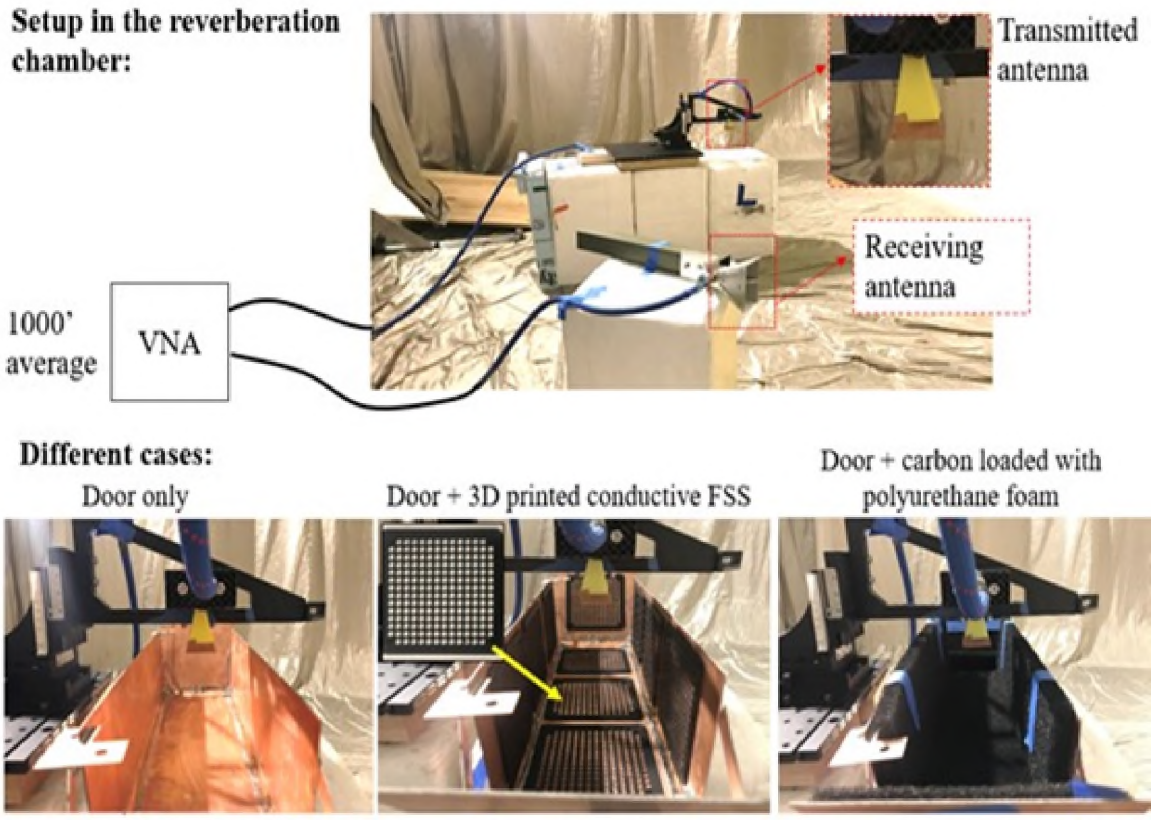

Figure 2.8. TRP Measurement Setup.

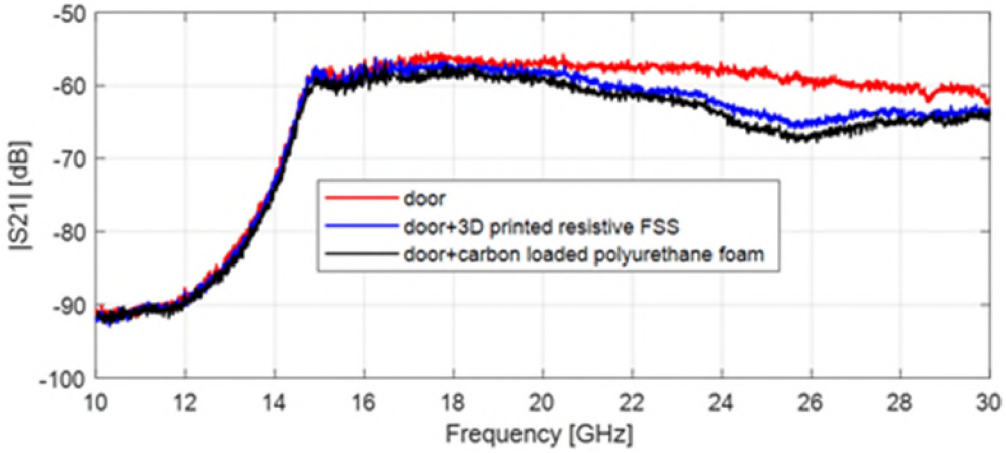

Figure 2.9. TRP Measurement Results.

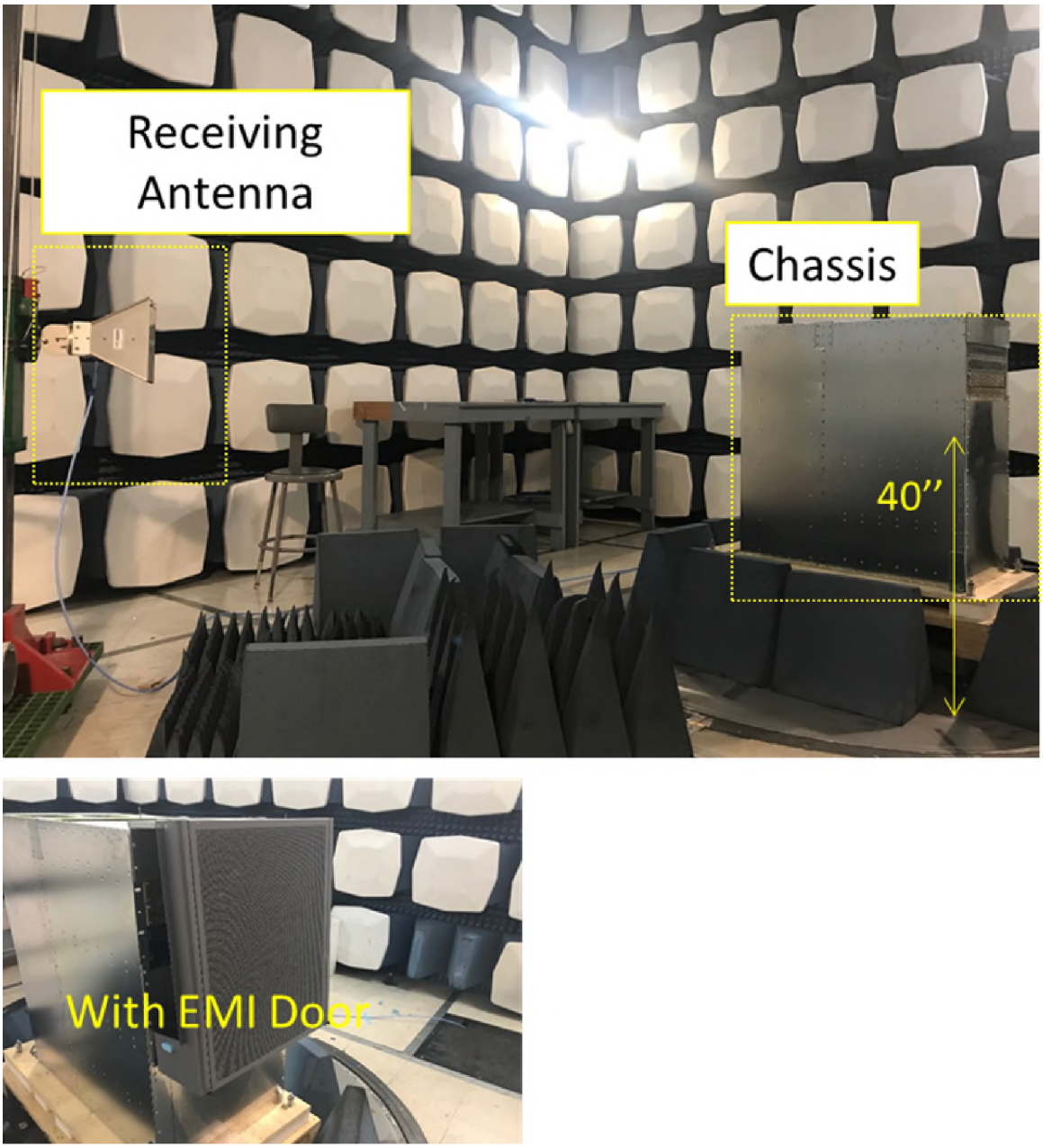

Figure 2.10. Router Rack Setup.

The picture of the designed source is shown in Figure 2.11. The structure is made by pressing a circular tube to an approximate rectangular waveguide. The left side of the tube is shorted by gasket. The other side of the tube is terminated by a slant absorber, minimizing the reflection at this side. The side wall of the waveguide is opened with many

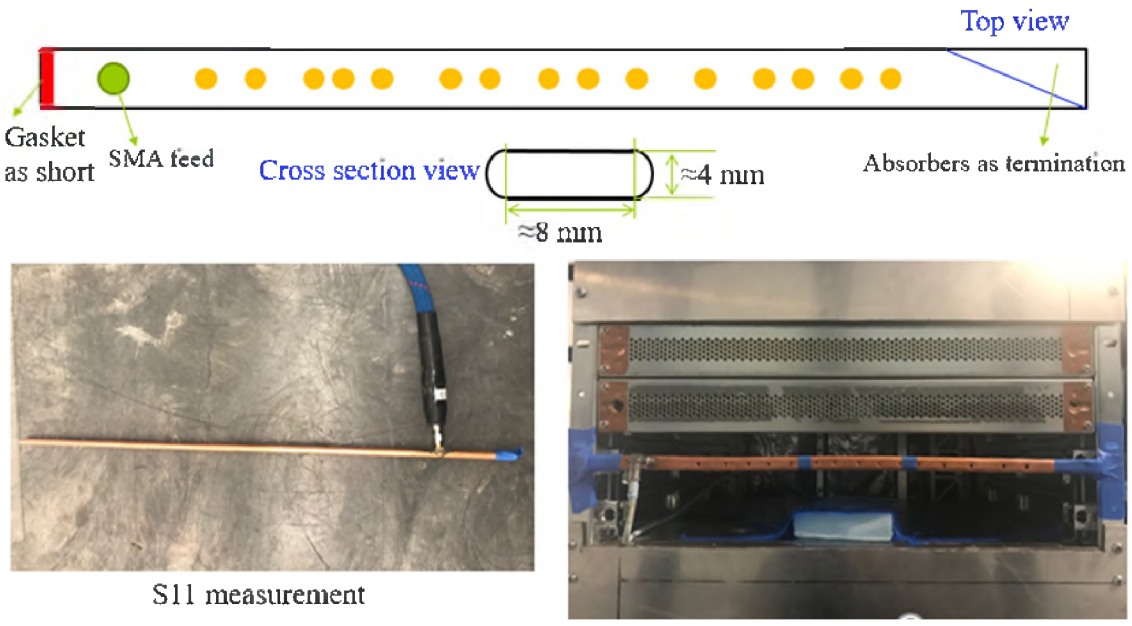

Figure 2.11. Self-Made Waveguide Source.

holes at random positions, which offers random-phase leakage from the waveguide to the outside similar to the emissions from the optical modules [18]. The feed of the waveguide is a SMA connector at the left side of the waveguide. A VNA is used to feed the waveguide with a sinusoidal signal at 26.5 GHz which is the working frequency of the optical modules. The waveguide source is suitable for mimicking the actual emission of a router system, as its radiation efficiency is very low, and the radiation pattern will have multiple peaks and nulls which is showing in the [18].

By measured the received power at a 2-meter distance (Figure 2.12), based on Equation 2.1:

$$E_{max} = P_{SA} + CableLoss + AntennaFactor + 107 \tag{2.1}$$

The maximum E-filed (Emax) could be estimated.

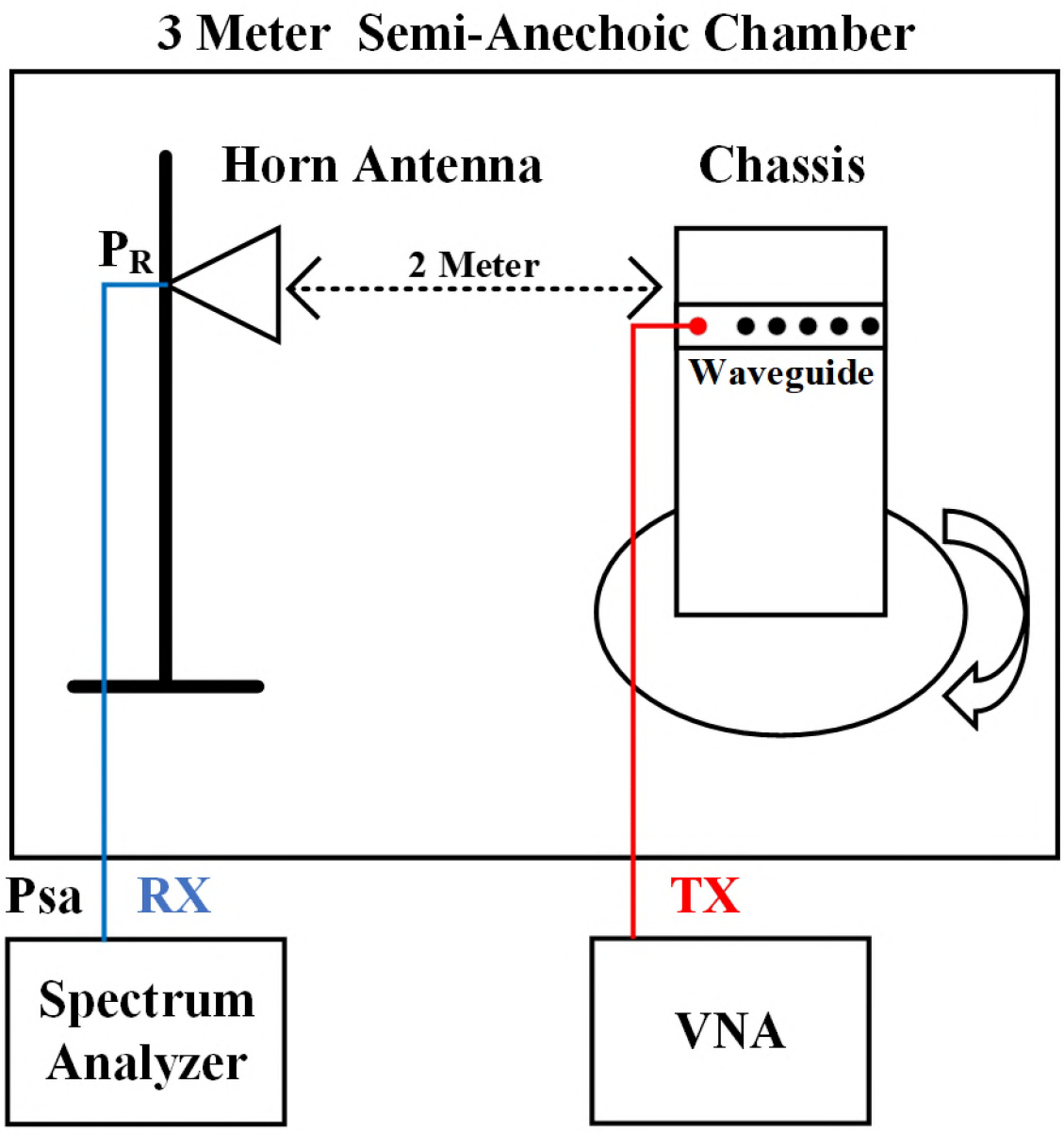

Figure 2.12. Radiated Emission Measurements Setup.

Addition of the EMI door leads to EM radiation scattering leading to a reduction of the maximum field due to a decrease of the directivity of the radiating source. By adding the absorber to the EMI door, an extra reduction of the EM radiation could be achieved. The configuration of the EMI door with absorber attached is showed in Figure 2.13.

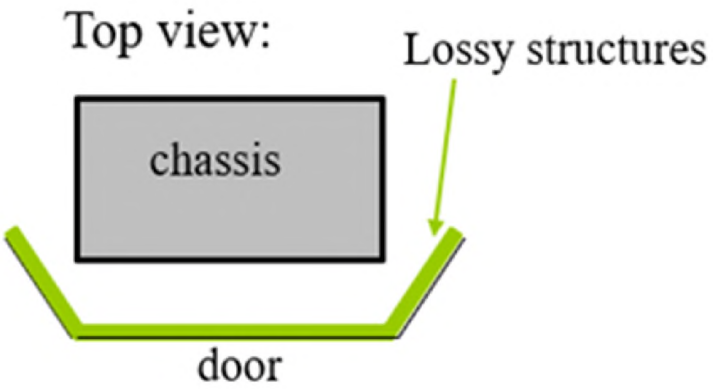

Figure 2.13. EMI Door Configuration During Emax Measurement.

Table 2.1. E_{max} Margin Measured on The Actual Application.

	E_{max} Reduction
Door	0 dB
Door + Carbon Loaded Foam (Commercial Absorber)	8.8 dB
Door + 3D Printed Conductive FSS	7.4 dB

By comparing the Emax reduction results achieved with the commercial absorber and the 3D printed FSS designed for the frequency range from 26 GHz to 27 GHz (Table 2.1), it can be seen that the 3D printed FSS is showing an attenuation level similar to a commercial absorber at the same time having lower price and better manufacturability.

3. SUMMARY AND CONCLUSIONS

This thesis introduces the methodology of manufacturing a frequency selective surface using conductive 3D printing filaments. It could easily design and tune for arbitrary absorption band because it has a periodic simple circular aperture FSS pattern.

The current design still has several problems which need further more investigation. The lossy FSS designed for 26.5 GHz shown less effectiveness in both reflection coefficient measurement and total radiation power measurement by comparing with simulation results. It might cause by the inaccuracies of the material characterization. When the thickness of The 3D printing FSS layer reduces to 0.6 mm, it is not stiff enough to hold the structure as design.

The 3D printed lossy FSS does provide a good absorption in the router system to reduce the radiation emission. With further more investigation on different FSS pattern designs, it can have a chance to provide better absorption by comparing with the commercial absorber.

REFERENCES

[1] Bruce Archambeault, Samuel Connor, and JC Diepenbrock. Time domain gating of frequency domain s-parameter data to remove connector end effects for pcb and cable applications. In *2006 IEEE International Symposium on Electromagnetic Compatibility, 2006. EMC 2006.*, volume 1, pages 199–202. IEEE, 2006.

[2] Jay H Barton, Cesar R Garcia, Eric A Berry, Rodolfo Salas, and Raymond C Rumpf. 3-d printed all-dielectric frequency selective surface with large bandwidth and field of view. *IEEE transactions on antennas and propagation*, 63(3):1032–1039, 2015.

[3] Qiang Chen, Di Sang, Min Guo, and Yunqi Fu. Frequency-selective rasorber with interabsorption band transparent window and interdigital resonator. *IEEE Transactions on Antennas and Propagation*, 66(8):4105–4114, 2018.

[4] ColorFabb. Copperfill, 2021. URL `https://colorfabb.com/copperfill`.

[5] Filippo Costa, Agostino Monorchio, and Giuliano Manara. Analysis and design of ultra thin electromagnetic absorbers comprising resistively loaded high impedance surfaces. *IEEE Transactions on Antennas and Propagation*, 58(5):1551–1558, 2010.

[6] Saptarshi Ghosh and Sungjoon Lim. A miniaturized bandpass frequency selective surface exploiting three-dimensional printing technique. *IEEE Antennas and Wireless Propagation Letters*, 18(7):1322–1326, 2019.

[7] Michel Joussemet. Novel devices and material characterization at mm wave and terahertz. Technical report, 2010.

[8] Keysight. *85071B Materials Measurement Software User's Manual (Apr93)*, 1993.

[9] R Kronberger and Volker Wienstroer. 3d-printed fss using printing filaments with enclosed metal particles. In *2017 Progress in Electromagnetics Research Symposium-Fall (PIERS-FALL)*, pages 808–811. IEEE, 2017.

[10] Xian Qi Lin, Peng Mei, Peng Cheng Zhang, Zhi Zhang David Chen, and Yong Fan. Development of a resistor-loaded ultrawideband absorber with antenna reciprocity. *IEEE Transactions on Antennas and Propagation*, 64(11):4910–4913, 2016.

[11] Yuanzhuo Liu, Ruijie He, Jiangshuai Li, and Victor Khilkevich. Measurement of the total radiated power contributions in a reverberation tent. In *2019 IEEE International Symposium on Electromagnetic Compatibility, Signal & Power Integrity (EMC+ SIPI)*, pages 654–657. IEEE, 2019.

[12] Pratik Maheshwari, Victor Khilkevich, David Pommerenke, Hamed Kajbaf, and Jin Min. Application of emission source microscopy technique to emi source localization above 5 ghz. In *2014 IEEE International Symposium on Electromagnetic Compatibility (EMC)*, pages 7–11. IEEE, 2014.

[13] Rui Mi, Wei Zhang, Kaustav Ghosh, Sameer Walunj, Qian Liu, Jacques Rollin, Philippe Sochoux, David Pommerenke, and Victor Khilkevich. A multi-mode noise reference source for verifying different conducted emission setups. In *2021 Joint IEEE International Symposium on Electromagnetic Compatibility, Signal & Power Integrity (EMC+ SIPI) and EMC Europe*. IEEE, 2021.

[14] Ben A Munk. *Frequency selective surfaces: theory and design*. John Wiley & Sons, 2005.

[15] Protopasta. Electrically conductive composite pla, 2021. URL `https://www.proto-pasta.com/products/conductive-pla`.

[16] MWB Silva, ALPS Campos, and LC Kretly. Design of thin microwave absorbers using lossy frequency selective surfaces. *Microwave and Optical Technology Letters*, 57(4):928–933, 2015.

[17] Jaroslav Zechmeister and Jaroslav Lacik. Complex relative permittivity measurement of selected 3d-printed materials up to 10 ghz. In *2019 Conference on Microwave Techniques (COMITE)*, pages 1–4. IEEE, 2019.

[18] Wei Zhang, Javad Soleiman Meiguni, Kaustav Ghosh, Abhishek Patnaik, Morten Sørensen, Ahmad Hosseinbeig, David Pommerenke, Jacques Rollin, Jing Li, Qian Liu, et al. System-level emi of an artificial router system with multiple radiators: Prediction and validation. *IEEE Transactions on Electromagnetic Compatibility*, 62 (4):1601–1610, 2020.

VITA

Rui Mi received the B.S. degree in electrical engineering from the Missouri University of Science and Technology, Rolla, MO, USA, in May 2019. He received the M.S. degree in Electrical Engineering from the Missouri University of Science and Technology, Rolla, MO, USA, in July 2021. He joined the Electromagnetic Compatibility Laboratory as graduate research assistant from 2019 to 2021.

His research interests included RF circuits, instrumentation, and electromagnetic interference measurement and design.